

Checkerboard charge density wave and pseudogap in high- T_c cuprates

Jian-Xin Li,^{1,2} Chang-Qin Wu,^{1,3} and Dung-Hai Lee^{1,4}

¹Department of Physics, University of California at Berkeley, Berkeley, CA 94720, USA

²National Laboratory of Solid State Microstructure, Nanjing University, Nanjing 210093, China

³Department of Physics, Fudan University, Shanghai 200433, China

⁴Material Science Division, Lawrence Berkeley National Laboratory, Berkeley, CA 94720, USA
(Dated: March 23, 2024)

We consider the scenario where a 4-lattice constant, rotationally symmetric charge density wave (CDW) is present in the underdoped cuprates. We prove a theorem that puts strong constraint on the possible form factor of such a CDW. We demonstrate, within mean-field theory, that a particular form factor within the allowed class describes the angle-resolved photoemission and scan tunneling spectroscopy well. We conjecture that the "large pseudogap" in cuprates is the consequence of this type of charge density wave.

I. INTRODUCTION

After almost two decades of experimental study, it is known that the high temperature superconductors have the following known ordered states: 1) antiferromagnetic order at very low doping ($x < 3\%$), 2) the d-wave superconducting (DSC) order for $5\% < x < 30\%$. While these two orders exist in all families of cuprates, there is a third order, namely, 3) a 4-lattice constant charge and 8-lattice constant spin density wave order, occurring near doping $x = 1/8$ in the $\text{La}_{1.48}\text{Nd}_{0.4}\text{Sr}_{0.12}\text{CuO}_4/\text{La}_{1.875}\text{Ba}_{0.125}\text{CuO}_4$ (LNSCO/LBCO) system¹. There is a wide-spread belief that this charge/spin density wave order is anisotropic, i.e., they form stripes^{1,2,3,4}.

A significant part of the high- T_c mystery lies in the behavior of the underdoped system⁵. Based on specific heat, nuclear magnetic resonance⁷, DC transport⁸, optical and Raman spectroscopy^{9,10}, angle-resolved photoemission (ARPES)¹¹ and tunneling^{12,13,14,15,16}, Tallon and Loram have made the case that the high- T_c superconductors possess two energy gaps, a pseudogap and a superconducting gap⁶. Recently ARPES experiments on LSCO system¹⁷ and underdoped Bi2212¹⁸ both point to a large pseudogap in the antinodal region and a superconducting gap near the Brillouin zone diagonals. Similar result has also been found in electronic Raman scattering experiment on Hg1201¹⁹. In addition, it is shown that for underdoped Bi2212 a large pseudogap exists in the antinodal region even at temperature $3T_c$, while a gapless Fermi arc exists near the nodes.²⁰

Recently, there are clear evidences from the scan tunneling spectroscopy (STM) studies suggesting the presence of a 4-lattice constant checkerboard order in NaCCOC¹⁴ and underdoped Bi2212^{15,16}. Interestingly ARPES study has shown that in $\text{Na}_x\text{Ca}_{2-x}\text{CuO}_2\text{Cl}_2$, where STM found checkerboard order¹⁴, the Fermi arcs survive²¹.

In view of these new experimental results we ask the question "can the pseudogap in underdoped cuprates be caused by some kind of checkerboard CDW?". To answer the question, we will look at the effects of the checker-

board CDW on low energy quasiparticles. Since the existence of low energy quasiparticles is an experimental fact, it is reasonable to model the influence of CDW by an effective scattering Hamiltonian of the form

$$H_{\text{CDW}} = \sum_{\mathbf{Q}, \mathbf{k}} \sum_{\mathbf{k}'} f(\mathbf{k}; \mathbf{Q}) C_{\mathbf{k}+\mathbf{Q}}^+ C_{\mathbf{k}} + \text{h.c.}; \quad (1)$$

where \mathbf{Q} is the CDW ordering wavevector and $f(\mathbf{k}; \mathbf{Q})$ the form factor.

In the following, we will first explore the symmetry property of the checkerboard CDW form factor using the experimentally observed STM patterns in Sec.II. In Sec.III, we compare the low energy ARPES and STM spectral functions generated by two representatives among the allowed form factors. Section IV is the summary.

II. TWO THEOREMS ABOUT $f(\mathbf{k}; \mathbf{Q})$

In Fig. 1 (a), we reproduce the STM dI/dV image of $\text{Na}_x\text{Ca}_{2-x}\text{CuO}_2\text{Cl}_2$ from Ref.14. This particular image is made at bias voltage 30 mV. However, the same checkerboard pattern was seen in a wide bias range 150mV \leq $V \leq$ 150mV. Experimentally, it was determined that such a checkerboard pattern contains \mathbf{Q} , where

$$\mathbf{Q} = (2\pi/4, 0); (0, 2\pi/4) \quad (2)$$

as its fundamental ordering wavevector. Hence we limit the \mathbf{Q} summation in Eq. (1) to those given by Eq. (2) and \mathbf{k} to the first Brillouin zone. In Fig. 1 (b), we reproduce the two-point correlation function of the observed image presented in Ref.14. From Fig. 1 (a,b) we construct a caricature in Fig. 1 (c) to capture the essence of the observed checkerboard. Interestingly, in each 4×4 unit cell there are two inequivalent centers about which the checkerboard is symmetric under

$$C_{4v} = \{E; C_2; \sigma_x; \sigma_y; C_4; C_4^3; \sigma_{x+y}; \sigma_{x-y}\} \quad (3)$$

the point group of the square lattice. (Here E represents identity, and $C_{2,4}$ denote 180 and 90 degree rotations,

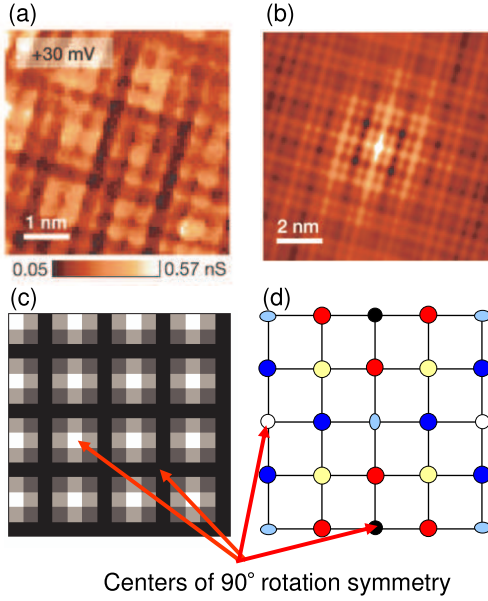


FIG. 1: (Color online) STM dI/dV map (a) and the autocorrelation image of $E_j < 100$ meV LDOS maps (b) from Hanaguri et al.¹⁴ on NaCCOC , showing the 4×4 ordering. (c) Caricature of the observed image shown in (a). (d) Possible LDOS pattern which exhibits 6 independent intensities in the 4×4 unit cell. In panels (c) and (d), two nonequivalent s-symmetry centers are indicated by arrows. In panel (d), the d-symmetry centers are indicated by the ellipses.

and denotes reflection.) In the following, we take this as implying that H_{CDW} is C_{4v} -invariant about these two centers.

Theorem I A CDW that has the ordering wavevectors given by Eq. (2) and possesses a center of C_{4v} symmetry in its unit cell must have the following properties.

(1) There must exist another inequivalent C_{4v} center in the unit cell. This second center is displaced from the first by the $(2,2)$ translation or its equivalent. About these two centers $f(\mathbf{k}; \mathbf{Q})$ has s-symmetry.

(2) There must exist two other centers around which H_{CDW} remains invariant under C_{2v} , the subgroup formed by the first four elements of C_{4v} , but changes sign under $C_4; C_4^3; x+y; x-y$. Spatially these two new centers must be displaced from the two C_{4v} centers by the $(2,0)$ and $(0,2)$ translation or their equivalents. About these two centers $f(\mathbf{k}; \mathbf{Q})$ has d-symmetry.

Proof. Let us assume H_{CDW} is invariant under C_{4v} at the origin, i.e., $R H_{\text{CDW}} R^{-1} = H_{\text{CDW}}$ where $R \in C_{4v}$. This implies

$$f(R\mathbf{k}; R\mathbf{Q}) = f(\mathbf{k}; \mathbf{Q}) \quad (4)$$

from Eq.(1). After a translation \mathbf{t} the form factor changes to

$$f(\mathbf{k}; \mathbf{Q}) \rightarrow g(\mathbf{k}; \mathbf{Q}) = f(\mathbf{k}; \mathbf{Q}) e^{i\mathbf{Q} \cdot \mathbf{t}}; \quad (5)$$

where \mathbf{t} can be any one of the 16 possible displacements within the unit cell

$$\mathbf{t} = (m; n); m, n = 0; 1; 2; 3; \quad (6)$$

Due to the fact that \mathbf{Q} only takes one of the four possible values given in Eq. (2) it can be easily checked that for $\mathbf{t} = (2; 2)$

$$g(R\mathbf{k}; R\mathbf{Q}) = g(\mathbf{k}; \mathbf{Q}) \quad 8R \in C_{4v}; \quad (7)$$

and for $\mathbf{t} = (2; 0); (0; 2)$

$$\begin{aligned} g(R\mathbf{k}; R\mathbf{Q}) &= g(\mathbf{k}; \mathbf{Q}) \quad R \in C_{2v} \\ g(R\mathbf{k}; R\mathbf{Q}) &= -g(\mathbf{k}; \mathbf{Q}) \quad R \in C_{4v} \setminus C_{2v}; \end{aligned} \quad (8)$$

where $C_{4v} \setminus C_{2v} = \{C_4, C_4^3; x+y; x-y\} \subset C_{4v}$.

Theorem I implies that any 90-degree rotationally symmetric CDW with $(2\pi/4; 0); (0; 2\pi/4)$ ordering wavevectors must simultaneously possess s-symmetry centers and d-symmetry centers. The presence of both symmetry centers is a necessary consequence of the CDW being rotationally symmetric. This fact was overlooked in the earlier version of this paper. Conversely any four lattice constant CDW that does not possess both symmetry centers must break rotation symmetry. In addition, it can be shown easily that a rotationally symmetric CDW discussed above possesses 6 inequivalent sites in the unit cell²², hence allowing 6 different values of dI/dV . This is shown in Fig. 1 (d).

Theorem II If H_{CDW} is time reversal invariant, $f(\mathbf{k}; \mathbf{Q})$ must be real if one chooses either d- or s-symmetry center as the origin.

Proof. Time reversal symmetry requires

$$f(\mathbf{k}; \mathbf{Q}) = f(\mathbf{k}; -\mathbf{Q}); \quad (9)$$

Since $f(\mathbf{k}; \mathbf{Q})$ is invariant under the 180 degree rotation about the s and d centers we have

$$f(\mathbf{k}; \mathbf{Q}) = f(-\mathbf{k}; -\mathbf{Q}); \quad (10)$$

As a result,

$$f(\mathbf{k}; \mathbf{Q}) = f(\mathbf{k}; \mathbf{Q}); \quad (11)$$

i.e, $f(\mathbf{k}; \mathbf{Q})$ is real. QED

III. EFFECTS OF THE CDW ON ARPES AND STM SPECTRA

In this section we apply the two theorems proven above and take the input from a previous renormalization group calculation²³ to guess the plausible form of $f(\mathbf{k}; \mathbf{Q})$. We then investigate the effect of the checkerboard CDW on the STM and ARPES spectral functions of the low energy quasiparticles. We stress that the purpose of this

section is not to prove that the ground state of certain microscopic Hamiltonian has CDW order. Rather, we take a phenomenological approach by assuming its existence and look at its consequences that are observable by STM and ARPES.

In Ref.23 it was shown that, with the help of electron-phonon interaction, a class of electron-electron scattering is enhanced at low energies. This class of scattering involves (momentum conserving) scattering of a pair of quasiparticles near the antinodes. For example, consider a pair of quasiparticles lying on the opposite sides of the almost nested Fermi surface near the $(\pi; 0)$ antinodes as shown in Fig 2 (a). After the scattering these two quasiparticles switch sides. The momentum transfer in such a scattering is the "nesting wavevector" of the antinodes. For systems such as NaCCOC²¹ and underdoped Bi2212²⁴ it has been shown that such nesting wavevectors are approximately given by Eq. (2). Interestingly, Ref.23 also shows that accompanying each such scattering there is a related process, whose scattering amplitude has opposite sign, where one of the quasiparticle scattering takes place near the $(0; \pi)$ rather than the $(\pi; 0)$ antinode [Fig 2 (b)]. It was also noticed that when this type of quasiparticle scattering grows strong it tends to drive a CDW whose form factor has the property that

$$\text{sign}[f(\mathbf{R}; \mathbf{k}; \mathbf{Q})] = \text{sign}[f(\mathbf{k}; \mathbf{Q})] \text{ for } \mathbf{R} \in C_{4v} \cup C_{2v} \quad (12)$$

In the following, let us choose the d-symmetry center as the origin. Thus

$$f(\mathbf{R}; \mathbf{k}; \mathbf{R}; \mathbf{Q}) = f(\mathbf{k}; \mathbf{Q}) \text{ for } \mathbf{R} \in C_{4v} \cup C_{2v} \quad (13)$$

Combine Eq. (13) with Eq. (12) we obtain

$$\text{sign}[f(\mathbf{k}; \mathbf{R}; \mathbf{Q})] = \text{sign}[f(\mathbf{k}; \mathbf{Q})] \text{ for } \mathbf{R} \in C_{4v} \cup C_{2v} \quad (14)$$

In addition, Eq. (12) plus the continuity condition requires

$$f(\mathbf{k}; \mathbf{Q}) = 0 \text{ for } \mathbf{k} \text{ along } \hat{x} \text{ or } \hat{y} \quad (15)$$

The above considerations lead us to the following ansatz for the CDW form factor

$$f(\mathbf{k}; \mathbf{Q}) = S_k(\mathbf{Q})(\cos k_x - \cos k_y) - S_k(\mathbf{Q})f_0(\mathbf{k}); \quad (16)$$

where $S_k(\mathbf{Q}) > 0$. In the following we shall pick a simple realization of Eq. (16) and focus on \mathbf{k} lying close to the Fermi surface.

In general the CDW couples each \mathbf{k} to other 15 \mathbf{k} points in the first Brillouin zone. However, most of these 16 \mathbf{k} 's lie far away from the Fermi surface, hence can be omitted in the low-energy theory. This suggests that one only needs to keep a few close neighbors for each \mathbf{k} . Another important consideration guiding our construction of H_{CDW} is the requirement that a robust antinodal CDW gap exists for reasonable change of doping. It turns out that this requirement is satisfied as long as the nested scattering across the antinodal Fermi surface is the dominant scattering process.

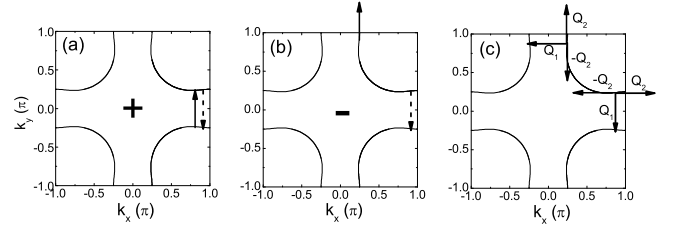


FIG. 2: The two enhanced sets of electron-electron scattering (panels (a) and (b)), as obtained from a renormalization group calculation²³. The scattering amplitude between these two sets differs by a sign. (c) The CDW-induced quasiparticle scatterings (only those in the first quadrant of the Brillouin zone are shown). The solid lines in these figures represent the normal state Fermi surface.

Put all the constraints together we consider the following quasiparticle Hamiltonian in the absence of superconducting pairing

$$H = \sum_{\mathbf{k}} \epsilon_{\mathbf{k}} c_{\mathbf{k}}^\dagger c_{\mathbf{k}} + \sum_{\mathbf{k}} A(\mathbf{k}) c_{\mathbf{k}}^\dagger c_{\mathbf{k}+\mathbf{Q}} + \text{h.c.} \quad (17)$$

where

$$A(\mathbf{k}) = (c_{\mathbf{k}}^\dagger; c_{\mathbf{k}+\mathbf{Q}_1}^\dagger; c_{\mathbf{k}+\mathbf{Q}_2}^\dagger; c_{\mathbf{k}-\mathbf{Q}_2}^\dagger); \quad (18)$$

and

$$A(\mathbf{k}) = \begin{pmatrix} 0 & S_0 f_0(\mathbf{k}) & S_1 f_0(\mathbf{k}) & S_2 f_0(\mathbf{k}) \\ S_0 f_0(\mathbf{k}) & 0 & 0 & 0 \\ S_1 f_0(\mathbf{k}) & 0 & 0 & 0 \\ S_2 f_0(\mathbf{k}) & 0 & 0 & 0 \end{pmatrix} \quad (19)$$

In Eq. (19)

$$Q_1 = \text{sign}(k_x)(2; -4; 0); Q_2 = (0; 2; -4) \text{ for } |k_x| < |k_y| \\ Q_1 = \text{sign}(k_y)(0; 2; -4); Q_2 = (2; -4; 0) \text{ for } |k_x| > |k_y|$$

as shown schematically in Fig 2 (c). In addition, we expect S_0 to be stronger than S_1 and S_2 . For the normal state dispersion, we use $\epsilon_{\mathbf{k}} = t_0 + t_1 [\cos(k_x) + \cos(k_y)] + t_2 \cos(k_x) \cos(k_y) + t_3 [\cos(2k_x) + \cos(2k_y)] + t_4 [\cos(2k_x) \cos(k_y) + \cos(2k_y) \cos(k_x)] + t_5 \cos(2k_x) \cos(2k_y)$, with the hopping constants (in eV) $(t_1; \dots; t_5) = (0.5951; 0.1636; 0.0519; 0.1117; 0.0510)$ ²⁵. In the following, we will compare the effects of the CDW for the two cases where the Fermi surface is nested/not nested by the \mathbf{Q} given by Eq. (2). (We adjust t_0 to control the degree of nesting.) As to the CDW order parameter, we choose

$$S_0 = s_c; S_1 = s_c; S_2 = s_c \quad (20)$$

We first discuss the case with Fermi surface nesting. In Fig 3 (a) and (c) we present the real-space dI/dV image at bias voltage 20 mV and the ARPES intensity map at the

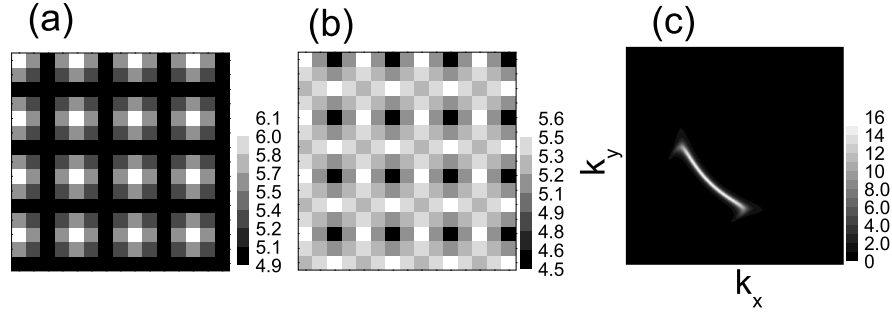


FIG. 3: Panel (a) and (b) are the dI/dV in q space for the CDW state where the $f_0(\mathbf{k})$ in Eq. (17) and Eq. (19) is $\cos k_x - \cos k_y$ and $j\cos k_x - \cos k_y$, respectively. The window of view is 15×15 lattice unit cells. Panel (c) is their Fermi energy ARPES intensity maps (Both form factors give the same intensity map). Here only the first quadrant of the Brillouin zone is shown. In making these figures we have chosen ϕ_0 to produce a 60 meV gap at the antinodes. The parameters in Eq. (20) is chosen to be 0.2. A quasiparticle energy broadening of 10 meV and a $t_0 = 0.0945$ eV are used.

Fermi level. These results are calculated with $s = 0.2$ in Eq. (20). The primary effect of changing s is to 1) change the intensity variation in the black perimeter in each unit cell in Fig.3(a); and 2) affect the strength of shadow band in Fig.3(c) (see later). Except these changes, the main features of both results are preserved. In Fig.3(b) we show the dI/dV in q space resulting from Eq. (17) where the $f_0(\mathbf{k})$ in Eq. (19) is replaced by $j\cos k_x - \cos k_y$ (Of course, after such a choice the d -symmetry center becomes the s -symmetry center). The purpose of this figure is to demonstrate the sensitivity of the real space image on the sign of f_0 . Indeed, while the ARPES image is completely unaffected by such a change, the real space dI/dV is strongly modified. Upon a comparison with the checkerboard pattern observed in $\text{Na}_x\text{C}_{2-x}\text{CuO}_2\text{Cl}_2$ ¹⁴, it is clear that the form factor $\cos k_x - \cos k_y$ (Fig.3(a)) produces the real space description best. To better understand the Fermi arc present in Fig.3(c) we note that in the presence of CDW, the new Fermi surface is determined by

$$\det[A(\mathbf{k})] = 0: \quad (21)$$

Since $\det[A(\mathbf{k})]$ is real (because $A(\mathbf{k})$ is Hermitian) $\det[A(\mathbf{k})] = 0$ yields a single equation with two unknowns (k_x and k_y). Generically, one expects the solutions to form closed one-dimensional curves. Since $f_0(\mathbf{k})$ vanishes at the node, it is natural to expect the Fermi surface to be practically unaffected in its vicinity. Such an unaffected piece of the Fermi surface and its CDW shadows form a closed contour. The reason that in Fig.3(c) only a Fermi arc is visible is due to the CDW coherence factor²⁶. In Fig.3(c), the strongest shadow band effect shows up near the end of the Fermi arcs. Note that such shadow band position is very different from that expected from antiferromagnetism. Presently there is no report of seeing such shadow bands^{20,27}. The reason may be: 1) the CDW correlation length as observed by STM experiment is not sufficiently long (It is typically of 10 nanometers); 2) in the pseudogap regime, the superconducting pairing still persists. In all cases we studied, the superconducting

pairing is very effective in weakening the shadow band effect. When moving away from the zero binding energy, we find that the main changes in the ARPES intensity map are: 1) the intensity in the antinodal regions increases, and 2) the Fermi arcs shrink and move towards the origin of the first Brillouin zone.

By considering all panels of Fig.3, it is obvious that it is the checkerboard CDW with $f_0(\mathbf{k}) = \cos k_x - \cos k_y$ that reproduces both the ARPES and STM phenomenology well. Therefore, we will only consider this kind of form factor in the rest of the paper.

Now, we turn to the case without Fermi surface nesting. In this case, using the checkerboard CDW with an order parameter of the same magnitude as that in Fig.3, we obtain a weaker fragmentation of the Fermi surface as shown in Fig.4(a). As to the real space pattern (not shown), the only difference with Fig.3(b) is a slight increase in the intensity variation in the dark perimeter region.

Next, we turn on a DSC pairing and ask what is the signature of the checkerboard CDW and superconducting pairing coexistence in STM. In this case the Hamiltonian becomes

$$H = \sum_{\mathbf{k}} \begin{pmatrix} X & \\ & \end{pmatrix} + (\mathbf{k})H(\mathbf{k}) - (\mathbf{k}); \quad (22)$$

where

$$+ (\mathbf{k}) = \begin{pmatrix} + & \\ & \end{pmatrix} (\mathbf{k}); \quad \# (\mathbf{k}) ; \quad (23)$$

and

$$H(\mathbf{k}) = \begin{pmatrix} A(\mathbf{k}) & B(\mathbf{k}) \\ B(-\mathbf{k}) & A(-\mathbf{k}) \end{pmatrix} : \quad (24)$$

In the above equations

$$\begin{aligned} B_{ij}(\mathbf{k}) &= 0 \text{ for } i \neq j \\ B_{ii}(\mathbf{k}) &= \begin{matrix} k; & k+Q_1; & k+Q_2; & k-Q_2 \end{matrix} \text{ for } i = 1;2;3;4: \end{aligned} \quad (25)$$

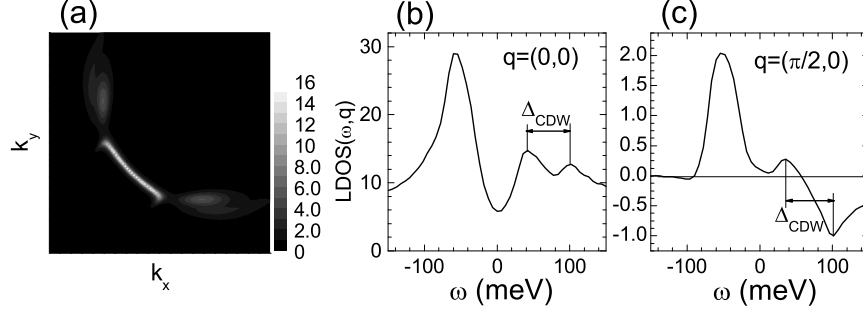


FIG. 4: (a) The ARPES intensity at E_F for the checkerboard CDW with the form factor $\cos k_x - \cos k_y$ and a 60 meV gap. (b) and (c) are the $q = (0;0)$ and $q = (\pi/2;0)$ Fourier components of LDOS for a state with a 60 meV CDW gap and a $\Delta_0 = 40$ meV DSC pairing parameter. A $t_0 = 0.1215$ eV is used.

For d-wave superconducting (DSC) pairing $\Delta_k = \Delta_0 (\cos k_x - \cos k_y) = 2$. In the presence of inversion symmetry ($A(-k) = A(k)$) the Hamiltonian in Eq. (24) can also be written as

$$H(k) = A(k) \sigma_3 + B(k) \sigma_1 \quad (26)$$

In that case because $H(k)$ anticommutes with σ_y the eigen spectrum is particle-hole symmetric. Under such condition the zero-energy eigenvectors are also eigenvectors of σ_y . As a result, the locus of zero energy satisfies

$$\det[A(k) - iB(k)] = 0 \quad (27)$$

Since this determinant is complex, setting its real and imaginary parts to zero gives two equations for the two unknown k_x and k_y . Consequently, one expects the solutions to be isolated points in the Brillouin zone. Thus with the DSC pairing the Fermi arc produced by checkerboard CDW is reduced to point gap nodes.

In Fig.4 (b) and (c) we consider the case where a 60 meV checkerboard CDW order parameter coexists with a $\Delta_0 = 40$ meV DSC pairing. Fig.4 (b) shows the spatial averaged local density of states (LDOS). Note that the CDW feature on the negative bias side is much weaker than that of the positive side. This is because it is overwhelmed by the density of states due to the van Hove singularity. The two peaks on the positive bias side are the original antinodal coherence peak split by the CDW order. We have checked that the energy separation between these peaks is proportional to the CDW order parameter. Another way to determine the strength of the CDW order is to Fourier transform LDOS at the CDW ordering wavevector. In Fig.4 (c), the real part of the $q = (\pi/2;0)$ component of LDOS is shown. The two peaks on the positive bias side of Fig.4 (b) now appear as a peak and an antipeak. Again, the distance between them is proportional to the CDW order parameter. Thus we propose that by studying the Fourier transformed LDOS, it is possible to extract the strength of CDW ordering.

In Fig.5 (a), we show several ARPES momentum distribution curves (MDC) along the momentum cut $(\pi/2; k_y) \rightarrow (\pi/2; -k_y)$ at three different energies in the presence of a checkerboard CDW state. (b) The energy gap along the normal state Fermi surface for the pure checkerboard CDW state (dashed curve) and a state with coexisting CDW and DSC order (solid curve). The form factor of the CDW is $\cos k_x - \cos k_y$ and the CDW parameters are the same as those in Fig.3.

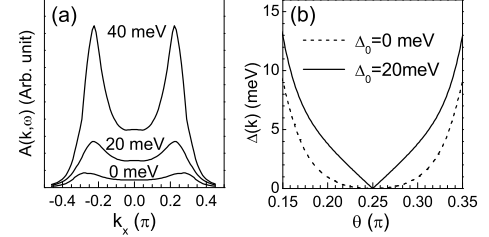


FIG. 5: (a) The ARPES MDC along the momentum cut $(\pi/2; k_y) \rightarrow (\pi/2; -k_y)$ at three different energies in the presence of a checkerboard CDW state. (b) The energy gap along the normal state Fermi surface for the pure checkerboard CDW state (dashed curve) and a state with coexisting CDW and DSC order (solid curve). The form factor of the CDW is $\cos k_x - \cos k_y$ and the CDW parameters are the same as those in Fig.3.

$(\pi/2; k_y) \rightarrow (\pi/2; -k_y)$ for the checkerboard CDW. All energies considered here are below the CDW gap. The presence of two non-dispersive MDC peaks separated by the CDW ordering wavevector is apparent. This is very similar to that observed in Ref.21.

In Fig.5 (b), we present the energy gap along the normal state Fermi surface for a pure checkerboard CDW state (dashed curve) and a state with both checkerboard CDW and DSC pairing (solid curve). The purpose of this figure is to illustrate the effect of DSC pairing in the pseudogap state. It shows how Fermi arc is replaced by a gap node. With thermal phase fluctuations, this explains why Fermi arcs shrink to four points as temperature approaches zero as observed recently²⁰. Given these results, we feel quite tempted to associate the larger checkerboard CDW gap with the large pseudogap and the smaller pairing gap on the Fermi arc with the small pseudogap.

In the literature it is widely believed that the pseudogap is a consequence of the short-range antiferromagnetic correlation⁵. Thus it is natural to ask what is the relation between the checkerboard CDW discussed above and such physics. On microscopic level the CDW presented in this paper represents the modulation in the hopping (or antiferromagnetic exchange) integrals. Consequently, it

is a kind of spin Peirls distortion which, of course, is compatible with the spin singlet pairing tendency of a quantum antiferromagnet. In addition to the above remarks we note that in a recent paper²⁸ it is found that checkerboard CDW is a self-consistent solution of a t - J like model at mean-field level, again testify that checkerboard CDW does not contradict the superexchange physics.

IV. CONCLUSION

In this paper, we present a symmetry constraint on the form factor of a 90 degree rotationally symmetric, commensurate, checkerboard charge density wave. Further guided by a previous renormalization group study²³ we construct a simple model describing the scattering of the low energy quasiparticles by the CDW. We then calculate the low energy ARPES and STM spectra using this simple model. The results compare favorably with the existing experiments. In particular, the results show a spatial dI/dV pattern similar to the one ob-

served in $\text{Na}_{1-x}\text{Ca}_x\text{CuO}_2\text{Cl}_2$ and underdoped Bi2212 by STM^{14,16}. Moreover, in the momentum space it produces Fermi arcs resembling those observed by ARPES^{17,21}. In the presence of a d -wave superconducting pairing, the Fermi arcs of the checkerboard CDW are reduced to four gap nodes²⁰. Therefore, this study supports the notion that the large antinodal pseudogap in underdoped cuprates is generated by the checkerboard charge density wave^{29,30,31} conjectured at the beginning of the paper.

V. ACKNOWLEDGEMENT

We thank Seamus Davis, Henry Fu, Gey-Hong Gweon, Alessandra Lanzara, and Zhi-Xun Shen for valuable discussions. JXL and CQW acknowledge the support of the Berkeley Scholar program and the NSF of China. DHL was supported by the Director, Office of Science, Office of Basic Energy Sciences, Materials Sciences and Engineering Division, of the U.S. Department of Energy under Contract No. DE-AC02-05CH11231.

-
- ¹ J.M. Tranquada et al, Nature (London) 375, 561 (1995).
 - ² J. Zaanen and O. Gunnarsson, Phys. Rev. B 40, 7391 (1989); K. Machida, Physica C 158, 192 (1989); M. Kato, K. Machida, H. Nakanishi and M. Fujita, J. Phys. Soc. Jpn. 59, 1047 (1990).
 - ³ V.J. Emery, S.A. Kivelson and J.M. Tranquada, Proc. Natl. Acad. Sci. 96, 8814 (1999).
 - ⁴ D. Reznik et al, Nature (London) 440, 1170 (2006).
 - ⁵ For a review, see, e.g., P.A. Lee, N. Nagaosa, and X.G. Wen, Rev. Mod. Phys. 78, 17 (2006).
 - ⁶ J.L. Tallon and J.W. Loram, Physica C 349, 53 (2001).
 - ⁷ M. Takigawa et al, Phys. Rev. B 43, 247 (1991).
 - ⁸ H. Takagi et al, Phys. Rev. Lett. 69, 2975 (1992).
 - ⁹ A.V. Puchkov, D.N. Basov, and T. Timusk, J. Phys. Condens. Matter 8, 10049 (1996); C. Bernhard et al, Phys. Rev. B 59, R 6631 (1999).
 - ¹⁰ G. Blumberg et al, Science 278, 1427 (1997).
 - ¹¹ For references see, e.g., A. Damascelli, Z. Hussain and Z. X. Shen, Rev. Mod. Phys. 75, 473 (2003).
 - ¹² I. Maggio-Aprile et al, Phys. Rev. Lett. 75, 2754 (1995).
 - ¹³ K. Lang et al, Nature (London), 415, 412 (2002).
 - ¹⁴ T. Hanaguri et al, Nature (London) 430, 1001 (2004).
 - ¹⁵ K.M. McElroy et al, Phys. Rev. Lett. 94, 197005 (2005).
 - ¹⁶ J.C. Davis, KITP talk, and Y. Kohsaka et al, to be published.
 - ¹⁷ Fujimori et al, Talk in M²S-HTSC, Dresden 2006.
 - ¹⁸ Z.X. Shen, Talk in M²S-HTSC, Dresden 2006.
 - ¹⁹ M.L. Tacon et al, Preprint to be published in Nature 2006.
 - ²⁰ A. Kanigel et al, cond-mat/0605499 (unpublished).
 - ²¹ K.M. Shen et al, Science 307, 901 (2005).
 - ²² A similar pattern with four inequivalent bonds was presented by K. Seo et al cond-mat/0604061 (unpublished).
 - ²³ H.C. Fu, C. Honerkamp and D.H. Lee, cond-mat/0509072, to appear in Euro. Phys. Lett.
 - ²⁴ D.L. Feng et al, Physica C 341-348, 2097 (2000).
 - ²⁵ M.R. Norman et al, Phys. Rev. B 52, 615 (1994).
 - ²⁶ S. Chakravarty, C. Nayak, and S. Tewari, Phys. Rev. B 68, 100504 (2003); C. Bena, S. Chakravarty, J.P. Hu, and C. Nayak, Phys. Rev. B 69, 134517 (2004).
 - ²⁷ U. Chatterjee et al, Phys. Rev. Lett. 96, 107006 (2006).
 - ²⁸ C. Li et al, Phys. Rev. B 73, 060501(R) (2006).
 - ²⁹ A similar proposal involving a different type of translation symmetry breaking state was made by S. Chakravarty et al, Phys. Rev. B 63, 094503 (2001).
 - ³⁰ An earlier proposal relating the properties of the pseudogap state with CDW can be found in C. Castellani, C. Di Castro, and M. Grilli, Phys. Rev. Lett. 75, 4650 (1995).
 - ³¹ For references of other charge/spin density wave proposals see, e.g., S.A. Kivelson et al, Rev. Mod. Phys. 75, 1201 (2003), and S. Sachdev, Rev. Mod. Phys. 75, 913 (2003).